

# XnODR and XnIDR: Two Accurate and Fast Fully Connected Layers For Convolutional Neural Networks

Jian Sun<sup>a</sup>, Ali Pourramezan Fard<sup>b</sup> and Mohammad H. Mahoor<sup>b</sup>

<sup>a</sup>Department Of Computer Science, University of Denver, 2155 E Wesley Ave, Denver, 80210, Colorado, USA

<sup>b</sup>Department Of Computer Engineering, University of Denver, 2155 E Wesley Ave, Denver, 80210, Colorado, USA

## ARTICLE INFO

### Keywords:

CapsNet  
XNOR-Net  
Dynamic Routing  
Binarization  
Xnorization  
Machine Learning  
Neural Network

## ABSTRACT

Although Capsule Networks show great abilities in defining the position relationship between features in deep neural networks for visual recognition tasks, they are computationally expensive and not suitable for running on mobile devices. The bottleneck is in the computational complexity of the Dynamic Routing mechanism used between capsules. On the other hand, neural networks such as XNOR-Net are fast and computationally efficient but have relatively low accuracy because of their information loss in the binarization process. This paper proposes a new class of Fully Connected (FC) Layers by xnorizing the linear projector outside or inside the Dynamic Routing within CapsFC layer. Specifically, our proposed FC layers has two versions, XnODR (Xnorizing Linear Projector Outside Dynamic Routing) and XnIDR (Xnorizing Linear Projector Inside Dynamic Routing). To test their generalization, we insert them into MobileNet V2 and ResNet-50 separately. Experiments on three datasets, MNIST, CIFAR-10, MultiMNIST validate their effectiveness. Our experimental results demonstrate that both XnODR and XnIDR help networks to have high accuracy with lower FLOPs and fewer parameters (e.g., 95.32% accuracy with 2.99M parameters and 311.22M FLOPs on CIFAR-10).

## 1. Introduction

With the advancement of new computing devices, Convolution - based Neural Networks (CNNs) show dominance in image classification due to the CNNs' powerful and efficient feature extraction ability. Despite their power, CNNs have some limitations in capturing the positional relation between features in images. For example, a face with randomly ordered eyes, ears, nose, mouth, and eyebrows will be wrongly recognized as a human face.

To address this problem, Sabour *et al.* proposed CapsuleNet (CapsNet) in 2017 [34]. They introduced a new concept called Capsule, a group of neurons whose activity vector represents the instantiation parameters of a specific type of entity such as an object or an object part. In better words, a capsule is a vector, where its length size means the possibility of the appearance of an object or an image property. Its direction represents the object's image property, such as location, shape, size, direction, etc. Capsule's direction is mutually exclusive to its length. To deploy Capsule, Sabour *et al.* took the idea of K-Means clustering, created a Dynamic Routing (DR) mechanism as the classifier, embedded it into the network's final FC layer, and called this new layer CapsFC layer.

The CapsFC layer contains the linear projector and the DR mechanism. It loads input capsules into linear projector firstly, then improves the accuracy by DR, an iterative structure (check Section 3.1 for more details about Dynamic Routing). The linear projector outside the DR mechanism takes 5-dimensional capsules as input variables, while the

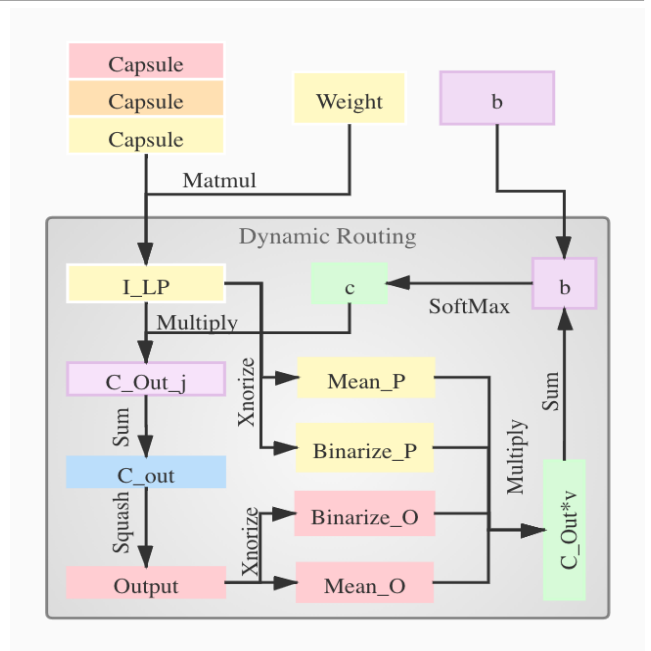


**Figure 1:** XnIDR(Xnor Inside Dynamic Routing), the Version 2 of proposed Fully Connected layer.

usual linear projector only accepts 2-dimensional flatten tensors. Dimension expansion causes the surge of parameters, multiplication and addition (MADD [35]) operations, and processing time. So does iteration. Therefore, compared with the usual FC layers, the CapsFC layer decreases the speed of both training and inference due to the dimension expansion and iterative structure. On the other hand, the lightweight models spend less time on network training and

Jian.Sun86@du.edu (J. Sun);  
Ali.Pourramezanfard@du.edu (A.P. Fard); mmahoor@du.edu  
(M.H. Mahoor)  
ORCID(s): 0000-0002-9367-0892 (J. Sun)

inference but perform as well as CapsNet. For example, Section.4 presents that MobileNet V2 [35] achieves 99.50% accuracy with the cost of 3.05M parameters when CapsNet reaches 99.65% accuracy with 6.80M parameters. As we can see, MobileNet V2's parameters are 50% less than CapsNet's. Furthermore, the network increasing parameters and its slow inference speed compromise the effect of CapsNet on mobile devices.

In terms of model speed, Rastegari *et al.* proposed a new approach called Xnorization [29], which is a simple, efficient, and accurate approximation to CNNs. It speeds the calculation by binarizing the input values and weights before convolution, introducing binary dot product with XNOR-Bitcounting operations, and using addition operation to replace multiplication operations during convolution. Rastegari *et al.* designed the XNOR-Net with the help of Xnorization. The experiment on MNIST [21] demonstrates that XNOR-Net can achieve high accuracy with fewer operations and faster speed. At the same time, the experiment also shows that XNOR-Net is more accurate than BWN (Binary Weight Network) on ImageNet [8] but is less compatible than full precision AlexNet because the binarization results in the network feature loss. Binarization takes the average values of each input channel as scaling factors. Such a straightforward method is too weak to depict complex datasets. Readers can find more discussion on Xnorization in Section.3.3 and Appendix.A. In general, XNOR-Net finishes classification tasks very well on small-scale datasets such as MNIST [21], but it is less satisfying on large-scale and complex datasets such as ImageNet [8]. ImageNet [8] usually requires a deep neural network, which has more convolution layers. However, the more layers XNOR-Net xnorizes, the more information it loses. Too much information loss brings obstacles for classification on small size images, small object images, or complex images. For example, [29] presents that XNOR-Net only results in 44.2% Top-1 accuracy on ImageNet [8]. Speed is important, but accuracy is also uncompromising.

Both CapsNet and XNOR-Net have pros and cons. Intuitively, we decide to define a layer to take the advantages from both networks. Thereby, this layer helps maintain comparable or achieve even higher accuracy like CapsNet while increasing the network speed like XNOR-Net. In better words, we would fuse the DR mechanism and Xnorization into the same FC layer.

In detail, the CapsFC layer runs the DR mechanism after linear projector, denoted by  $LP_{out}$ . In addition, there is another linear projector, denoted by  $LP_{in}$ , within the DR mechanism. Readers can find more details about  $LP_{in}$  in Section.3.1. We would xnorize  $LP_{out}$  and  $LP_{in}$  separately in our proposed FC layers to reduce parameters and FLOPs (floating point of operations).

In the meanwhile, we select to xnorize CapsFC layer because "fully connected layers can be implemented by convolution" [29]. Rastegari *et al.* converts xnorized convolution layer to fit FC layers [29]. Furthermore, it is key to xnorize the correct layers. For the sake of keeping as

much information as we could, we determine to xnorize the  $LP_{out}$  and  $LP_{in}$  separately and find that it barely affects the model's performance. We explain the reason in the Section.3.3. Finally, we get two different layers, XnODR (Xnor Outside Dynamic Routing) and XnIDR (Xnor Inside Dynamic Routing).

Moreover, to test the generalization of XnODR and XnIDR, we let them separately replace the usual FC layers of the typical lightweight model, MobileNet V2 [35]. So does the representative heavyweight model, ResNet-50 [14]. Finally, we validate these variants on MNIST [21], CIFAR-10 [20], and MultiMNIST [34] datasets. The experiment results present that XnODR and XnIDR are qualified to replace dense layers on the other models. Section.4 shows that both XnODR and XnIDR help speed the model and maintain comparable or even better accuracy.

Overall, the contributions of this paper are as follow:

- We propose a new Fully Connected Layer, called XnODR, by xnorizing the linear projection outside the dynamic routing.
- We propose a new Fully Connected Layer, called XnIDR, by xnorizing the linear projection inside the dynamic routing.
- XnODR and XnIDR suit both lightweight models and heavyweight models. In our experiments, we show that XnODR and XnIDR help get better accuracy with less FLOPs and less parameters by replacing the dense layers with XnODR or XnIDR on both MobileNet V2 [35] and ResNet-50 [14].

The remaining of the paper is organized as follows. Section.2 provides an overview of related work. Section.3 explains the new proposed FC layers. Section.4 introduces databases used in this work, presents the experimental configuration, evaluation metrics, the experimental results, and analysis. We discuss our work in Section.5 and finally conclude the paper in Section.6.

## 2. Related Work

### 2.1. Capsule Network

CNNs focus more on extracting features from images rather than orientational and relative spatial relationships between those features. Otherwise, the max-pooling layer helps CNNs to work surprisingly better than any previous models in many areas. Its good performance also covers CNNs' orientational and relative spatial relationships problem. However, the max-pooling layer still loses much valuable information. Sabour *et al.* [34] proposed CapsNet in 2017 to solve this problem, which consists of Convolutional layers, PrimaryCapsule layers, CapsFC layers, and a decoder<sup>1</sup>. The PrimaryCaps layer consists of convolutional operation and max-pooling. The CapsFC layer is similar

<sup>1</sup>This work focuses on the accuracy and speed of networks instead of the Decoder part

to the FC layer. They designed capsules and added a DR mechanism, which significantly improved the accuracy and interpretation of classification.

CapsNet inspires and motivates lots of papers. Researchers proposed novel methods by changing the original CapsNet. For example, Xi *et al.* proposed variants of CapsNet to explore better performance on complex datasets [39]. Lenssen *et al.* proposed group equivariant capsule networks to provide CapsuleNet solid equivariance and invariance property [22]. Bahadori implemented spatial coincidence filters in proposed spectral capsule networks to detect objects from features on a one-dimensional linear subspace [3]. Gu *et al.* improved the robustness of affine transformations and dropped the dynamic routing mechanism in Aff-CapsNets [12]. The above papers pay more attention to elevating the accuracy of the CapsNet.

Other researchers are exploring the various possibilities of CapsuleNet. For example, Lin *et al.* mixed CapsNet and scale-invariant feature transform (SIFT) and proposed CapsnetSIFT to address the visual distortion problem. This model can boost innate invariance to spacial-scale transformations [25]. Lin *et al.* proposed CTF-CapsNet, which takes advantage of both CapsNet and region proposal networks (RPNs), to provide good performance in Fine-grained image categorization [26]. Kim *et al.* explored the CapsuleNet's capability for text classification and proposed a novel statics routing mechanism to improve the results [18]. The above papers are devoted to extending CapsNet good performance to other tasks than purely image classification, such as detection, segmentation, fine-grained classification, and text classification.

In our work, we focus more on improving CapsNet's speed. CapsNet is time-consuming during training and inference, especially on complex datasets like CIFAR-10 [20], because of the DR's iterative structure. Moreover, it takes more time to perform convolution by multiplication. This paper presents a solution to address the low-speed performance of the CapsNet.

## 2.2. XNOR Network

CNNs' excessive parameters usually cause inefficient computation and memory utilization. Researchers proposed several methods to address this problem.

Firstly, Cybenko *et al.* [6], Seide *et al.* [46], Dauphin *et al.* [7], and Ba *et al.* [2] proposed theory of Shallow networks and did related experiments. The core idea of Shallow networks is to mimic deep neural networks to get similar numbers of parameters and similar accuracy. Otherwise, Shallow networks return less comparable accuracy on ImageNet [8].

It is also sensible to assemble CNNs with compact blocks that cost less memory and FLOPs. For example, several years ago, GoogleNet [36], ResNet [14], and SqueezeNet [17] achieved several benchmarks with the cost of fewer parameters by using the proposed new layers or structures. Recently, HGCNet [40] implements Hierarchical

Group Convolution to reduce error rate, which elevates representation capability by fusing feature maps from different groups.

Next, since that CNNs can achieve good performance without high precision parameters, quantizing parameters is another option for researchers. [11] quantized the weights of FC layers and stated that it only reduces by less than 10% in Top-1 accuracy on ILSVRC2012 by utilizing vector quantization techniques. The other quantization algorithms make progress in this field and achieve good performance too. For example, Hwang *et al.* designed a fixed-point network with ternary weights and 3-bits activations [16]. Lin *et al.* quantized each layer's representations by the back-propagation process and selected to only quantize neurons during the back-propagation process [24]. Floropoulos *et al.* proposed a novel vector quantization method by quantizing both the parameters and the activations with the minimum loss of accuracy [10]. The above papers present many different ways to quantize the framework.

Some researchers work on improving accuracy or speed with the given quantization methods. For example, Duarte *et al.* proposed a greedy path-following algorithm to quantize the weight of each layer, such as neurons or hidden units [28]. Touvron *et al.* presented a weight searching algorithm to search for discrete weights and avoid gradient estimation and non-differentiable problems to improve the accuracy during training the quantized deep neural network [43]. Wang *et al.* proposed a pruning algorithm to point out unnecessary low-precision filters and utilize Bayesian optimization to decide the pruning ratio [13]. These papers are very good, but less revolutionary than [11], [16], and [24].

Finally, Rastegari *et al.* proposed XNOR-Net in 2016 [29], which is different from the above methods. XNOR-Net uses standard deep architectures instead of shallow ones, trains networks from scratch rather than implementing pre-trained networks or networks with compact layers, and quantizes the weights and input values with two factors, +1, -1, instead of +1, 0, -1 [1]. Rastegari *et al.* stated that the usual CNNs would cost more time as the size of tensors increases due to multiplication and division operations performed in the convolutional calculations. To reduce the processing time and maintain the prediction accuracy, then, Rastegari *et al.* first created a binary version of CNN by binarizing weight values, which splits the weights into two parts, a sign matrix (spanned from 2 values {-1, 1}) and a scaling factor. They then proposed a new concept called Xnorization. Xnorization is to binarize both the input and weight values and obtain related sign matrices and scaling factors. Xnorization implements the XNOR operation to do the convolutional calculations. The advantage of the XNOR operation is that it uses plus and minus to do convolution rather than multiplication and division. Therefore, XNOR can save processing time substantially during the training time. They call the CNNs, XNOR-Net if it xnorize both the input and weights before doing convolution. It is worth

mentioning that according to [29], XNOR-Net has comparable performance on MNIST [21] and CIFAR10 compared to BNN(Binary Neural Network).

Other researchers also did a lot of work based on XNOR-Net. Yoshida *et al.* proposed Ternary Sparse XNOR-Net to improve accuracy and shrink the circuit size in FPGA (Field-programmable gate array) by ternarizing the weight data as  $(-1, 0, 1)$  [45]. Bulat *et al.* proposed XNOR-Net++ by fusing the activation's scaling factor, and weights in various ways to calculate their product under a given computation resource [4]. Liu *et al.* proposed Bi-Real-Net to improve the model's representational capability by using real-valued activations generated by each 1-bit convolution. Bi-Real-Net also helps address the training difficulty by utilizing a tighter approximation, a magnitude-aware binarization, a better initialization method, and a two-step scheme [27]. Zhu *et al.* proposed XOR-Net to offer a pipeline for binary networks both without and with scaling factors [47]. The above papers aim to reduce memory usage, speed up the inference time, and improve accuracy by creating different quantization methods or the new pipeline.

We also found that Xnorization causes the network to lose much information. Insufficient information prevents XNOR-Net from achieving as high accuracy as CNNs. In this work, we focus on improving accuracy. Our idea is to add a routing mechanism rather than modifying the sign, scaling factor, or the CNNs' main body. In this paper, CNNs' main body represents the CNNs without any FC layer.

### 2.3. Different Routing Mechanisms

In 2018, Hinton *et al.* [33] proposed EM (Expectation-Maximization algorithm) Routing. They obtain the pose matrix and output capsules' activation values by the iteration of EM Routing. EM Routing alternately calls Step E and Step M and fits the data into the Gaussian Mixture model. What's more, it converts the capsule from a 1-dimensional vector to a 2-dimensional pose matrix, which provides more related position information. Albeit EM routing looks so advancing, it becomes more time-consuming than the Dynamic Routing. People without many computing resources may hesitate to select EM Routing to train large-scale datasets such as ImageNet [8].

In 2020, Fabio *et al.* presented Variational Bayes (VB) Routing [32]. Compared with Dynamic Routing and EM Routing, it has more flexible control over capsule complexity by tuning priors to induce sparsity, and reducing the well-known variance-collapse singularities inherent to MLE-based mixture models such as EM. In general, VB Routing helps to overcome overfitting and unstable training issues found in EM Routing. However, researchers only validated VB Routing and EM Routing on small-scale datasets, such as MNIST [21] and CIFAR-10 [20], instead of the large-scale ones, such as ImageNet [8] or MS-COCO [23]. It would be more helpful if VB Routing helps reach solid accuracy on large-scale datasets too.

## 3. New Fully Connected Layer: XnODR and XnIDR

This section introduces the concept and steps to fuse the CapsFC layer and the Xnorization, which obtains the properties of high reasonableness and accuracy from CapsNet and the properties of fast inference speed from XNOR-Net. One of the proposed FC layers is XnODR, which does the binarization operation outside the dynamic routing. The other one is XnIDR, which does the binarization operation inside the dynamic routing. Both XnODR and XnIDR are modified based on CapsFC layer. They binarize the input and weights for the linear projector and speed up the network while maintaining comparable classification accuracy. For more details, we refer the reader to Section 3.3.

### 3.1. Dynamic Routing Review

Dynamic Routing [34] helps to activate core capsules and suppress unimportant ones from lower layers and highlight those core capsules with high probability. At the same time, as an iteration process, it improves the performance by iteratively updating the output capsules. It is used in XnODR and XnIDR as the routing mechanism too. Next, we describe its concept [34] in the following paragraphs.

Let  $\mathbf{C\_Out}_i$  denote the capsule  $i$  from lower layer  $l$ , and  $\mathbf{W}_{ij}$  denote the weight matrix between capsule  $i$  and  $j$ . Multiplying  $\mathbf{C\_Out}_i$  by  $\mathbf{W}_{ij}$  returns the prediction capsules  $\mathbf{C\_Out}_{j|i} = \mathbf{W}_{ij} \mathbf{C\_Out}_i$ .

Let  $b_{ij}$  denote initial logits, a log prior probability that capsule  $i$  should be coupled to capsule  $j$  from layer  $l + 1$ , and  $c_{ij}$  denote the importance of  $b_{ij}$  within all  $b_i$ , the sum of log prior probabilities that capsule  $i$  coupled to all capsule at layer  $l + 1$ . In other words,  $c_{ij}$  are coupling coefficients between capsule  $i$  and all the capsules in the layer above sum to 1, it measures the probability that  $\mathbf{C\_Out}_i$  activates  $\mathbf{C\_Out}_j$ . We formulate  $c_{ij}$  as:

$$c_{ij} = \frac{\exp(b_{ij})}{\sum_k \exp(b_{ik})} \quad (1)$$

Let  $\mathbf{C\_Out}_j$  denote the output of capsule  $j$  from layer  $l + 1$ . It is the weighted sum over all  $\mathbf{C\_Out}_{j|i}$  from the layer  $l$ , which can be formulated as:

$$\mathbf{C\_Out}_j = \sum_i c_{ij} \mathbf{C\_Out}_{j|i}. \quad (2)$$

Then **Squash** is an activation function like Relu, which controls the size of  $\mathbf{C\_Out}_j$  to be less than 1, and preserves its direction. This function is described in Eq.3:

$$\mathbf{v}_j = \frac{\|\mathbf{C\_Out}_j\|^2}{1 + \|\mathbf{C\_Out}_j\|^2} \frac{\mathbf{C\_Out}_j}{\|\mathbf{C\_Out}_j\|} \quad (3)$$

where  $\mathbf{v}_j$  represents the activated capsule, it is the vector output of capsule  $j$  and helps to update  $b_{ij}$ , which can be formulated as Eq.4:

$$b_{ij} = b_{ij} + \mathbf{C\_Out}_{j|i} \cdot \mathbf{v}_j. \quad (4)$$



The product of  $\mathbf{C\_Out}_{j|i} \cdot \mathbf{v}_j$  is large if there is a high correlation between the activated capsule and predicted capsule. A larger  $\mathbf{C\_Out}_{j|i} \cdot \mathbf{v}_j$  results to larger  $b_{ij}$ , which goes through softmax and helps to keep predict capsules which are highly correlated to activated capsules. Then, referring to Section.3.3, Eq.4 is the modified part in the new proposed XnIDR.

We summarise the above formulation to an iterative process called DR [34]. Iterative DR implements the property of local feature maps to calculate and decide whether or not to activate capsules, which is a substitute method. What's more, with the help of Capsules, DR takes the feature maps' location, direction, size, and other detailed information into consideration rather than simply detecting features such as CNNs. For example, we can make either a house or a sailboat with one square and one triangle. If we train the network by the house and test it on a sailboat, CNNs would wrongly classify it as a "house" since it only detects features independently. Oppositely, CapsNet with DR would activate related sailboat capsules, avoid mistakes after comprehensive analysis, and help to improve the prediction result,  $\mathbf{C\_Out}_i$ , by updating capsules in the FC layer. Section.3.3 provides the defection analysis of DR.

### 3.2. XnorNet Review

**Xnorization** and **XnorConvLayer** are two vital concepts introduced in [29] and used to define new Fully Connect layer. We refer the reader to Appendix.A and Appendix.B for more details. Next, we directly introduce XnODR and XnIDR in this section.

### 3.3. XnODR and XnIDR

A usual dense layer only has one linear projector, while the CapsFC layer has  $LP_{out}$  and  $LP_{in}$ , according to Section.1.  $LP_{in}$  is the product of prediction capsules from layer  $l$  to layer  $l+1$ , represented by  $\mathbf{C\_Out}_{j|i}$ , and the output of capsule  $j$  from layer  $l+1$  after squashing, represented by  $\mathbf{v}_j$ . On the other side, the input capsules get expanded from three dimensions to five dimensions before loading into  $LP_{out}$ . Otherwise, the input tensors of the usual dense layer only have two dimensions. Therefore, the CapsFC layer's linear projector costs more MADD [35] operations than the original dense layer. That is the reason why the CapsFC layer is time-consuming. In addition, the DR mechanism, as an iterative structure, provides more trainable parameters, which contributes to enlarging disparity on MADD from usual dense layer and spending more time on inference. In simple words, to seek implicit information, DR trades off accuracy with speed. For example, CapsNet achieves a Top-1 error rate of less than 0.5% on the small-scale and simple dataset, such as MNIST.

Given that the convolution layer can fulfill the function of the FC layer, we also use binarized data in the FC layer in the XNOR-Net. Binarization is a very convenient function. However, it averages the pixel values among each channel as a scaling factor that breaks the hierarchy of pixel values and fails to collect many implicit features. Furthermore, it only approximates the pixels simply by the product of sign

matrix and scaling factor, which exacerbates the information loss, a very apparent negative influence. In brief, XNOR-Net trades off speed with accuracy. Thereby, Xnorization at different layers aggravates the network's information loss, which prevents XNOR-Net from performing well like CNNs. This disparity is minor on small-scale and simple datasets but is apparent on large-scale complex datasets such as Imagenet [8] and AffectNet [31]. For example, in ImageNet [8], compared with 56.6% Top-1 accuracy at the usual AlexNet, AlexNet with Xnorization only achieves 44.2% top1 accuracy, which warns us of the importance of xnorizing the correct layers. The network accuracy will be closer to full precision models accuracy if we only xnorize the final dense layer instead of the second convolution layer. The reason is that the network already extracts enough feature maps before the last Dense layer and loses less information than xnorizing the second layer, where the network exactly starts mining feature maps.

Based on the above introduction, CapsNet is accurate but slow, Xnor-Net is fast but less accurate. Intuitively, we take DR from CapsuleNet and Xnorization from XNOR-Net and fuse them to create a new FC layer, a more accurate and faster layer. During the training and inference, this layer helps simplify operations and speed up the model by implementing Xnorization. It also helps maintain a comparable prediction accuracy by taking advantage of Capsules and DR to extract the direction, location, and other sophisticated information among feature maps. What's more, the new FC layer would do binarization before linear projector, replace multiplications with additions and subtractions, and do xnorization either outside or inside the DR mechanism. In summary, it has two different versions.

Before introducing our work, we summarise the CapsFC layer as the following.

Let  $\mathbf{I}_{Prim}$  denote output tensors from the PrimaryCap layer, with the size  $[b, caps\_in, dim\_in]$ ,  $\mathbf{I}_{Cap}$  denote input capsules, with the shape  $[b, caps\_in, caps\_out, 1, dim\_in]$ , where  $b$  represents batch size of input value;  $caps\_in$  represents the number of capsules loaded into this layer;  $caps\_out$  represents the number of capsules output from this layer; 1 represents that the capsule is a 1-dimensional vector;  $dim\_in$  represents the element number of this each input capsule. Then let  $\mathbf{W}_{Cap}$  denote weight, with the size  $[caps\_in, caps\_out, dim\_in, dim\_out]$ ,  $\mathbf{Bias}_{Cap}$  denote bias, with the size  $[caps\_in, caps\_out, 1, dim\_out]$ , where  $dim\_out$  represents the dimension of each output capsule.

We first expand  $\mathbf{I}_{Prim}$  to  $\mathbf{I}_{Cap}$ , then multiply  $\mathbf{I}_{Cap}$  by  $\mathbf{W}_{Cap}$  returns the product,  $\mathbf{I}_{LP}$ , next load  $\mathbf{I}_{LP}$  into DR:

$$\begin{aligned} \mathbf{I}_{LP} &= \mathbf{I}_{Cap} * \mathbf{W}_{Cap} \\ \mathbf{Y} &= \text{Dynamic\_Routing}(\mathbf{I}_{LP}) \end{aligned} \quad (5)$$

where  $\mathbf{I}_{LP}$  has the size  $[b, caps\_in, caps\_out, 1, dim\_out]$ ,  $\mathbf{Y}$  is the output of the Fully Connected layer. Its size is  $[b, 1, caps\_out, 1, dim\_out]$ . Next, we will discuss our work.

**XnODR(Xnor Outside Dynamic Routing):**  $\mathbf{I}_{Cap}$ , expanded from  $\mathbf{I}_{Prim}$ , is different from standard tensors with

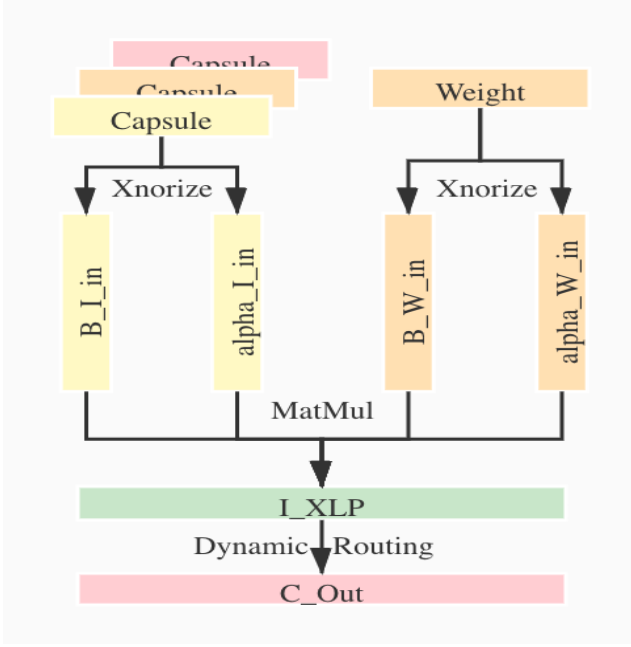


**Figure 2:** XnODR (Xnor Outside Dynamic Routing), the Version 1 of proposed Fully Connected layer.

the shape  $[num\_samples, flatten\_features]$ . We will get an accurate binary filter if we xnorize  $\mathbf{I}_{Cap}$  and its weight directly before the linear projector. However, we will also get an inaccurate scaling factor if we calculate average value cross all dimensions, such that dimension 0, 1, and 2 of  $\mathbf{W}_{Cap}$  denote weight, with the shape of  $[caps\_in, caps\_out, dim\_in, dim\_out]$ . Moreover, the linear projector is to change the size of the capsule vector from  $[1, dim\_in]$  to  $[1, dim\_out]$ . Inspired by this idea, we design a function, **XLP**, to address this problem by decomposing tensors and Xnorize linear project the inner two dimensions, and formulate them in Eq.6:

$$\begin{aligned} \mathbf{I}_{in}, \mathbf{W}_{in} &= Scan(Scan(Scan(\mathbf{I}_{Cap}), \mathbf{W}_{Cap})) \\ \mathbf{I}_{in} * \mathbf{W}_{in} &\approx (\mathbf{B}_{I_{in}} \otimes \mathbf{B}_{W_{in}}) \odot \alpha_{I_{in}} \alpha_{W_{in}} \\ \mathbf{I}_{XLP}[p, i, j, :, :] &= \mathbf{I}_{in} * \mathbf{W}_{in}, p \in [0, b], \\ i &\in [0, caps\_in], j \in [0, caps\_out]. \end{aligned} \quad (6)$$

where  $\mathbf{I}_{in}$  represents the inner two dimensions of  $\mathbf{I}_{Cap}$  with the shape  $[1, dim\_in]$ ,  $\mathbf{W}_{in}$  represents the inner 2 dimensions of  $\mathbf{W}_{Cap}$  with the shape  $[dim\_in, dim\_out]$ ,  $\mathbf{B}_{I_{in}}$  denotes the binary filter of  $\mathbf{I}_{in}$ ,  $\otimes$  denotes the convolutional operation using XNOR and the bitcount operations,  $\alpha_{I_{in}}$  denotes the scaling factor of  $\mathbf{I}_{in}$ ,  $\mathbf{B}_{W_{in}}$  denotes the binary filter of  $\mathbf{W}_{in}$ ,  $\alpha_{W_{in}}$  denotes the scaling factor of  $\mathbf{W}_{in}$ ,  $\mathbf{I}_{XLP}[p, i, j, :, :]$ 's size is  $[1, dim\_out]$ . Moreover, **Scan** function is to unpack the tensors on dimension 0 repeatedly until the inner two dimensions, because we hope to change the capsule vector from  $[1, dim\_in]$  to  $[1, dim\_out]$ .

Next step, we put the **XLP**'s output,  $\mathbf{I}_{XLP}$  with the shape  $[b, caps\_in, caps\_out, 1, dim\_out]$ , into DR mechanism to

get final output,  $\mathbf{Y}$ :

$$\mathbf{Y} = Dynamic\_Routing(\mathbf{I}_{XLP}). \quad (7)$$

The detail of DR mechanism is introduced in Section.3.1. According to the [29], the total number of operations in a standard convolution is  $cN_W N_I$ , where  $c$  is channel number,  $N_W = wh$ ,  $N_I = w_{in}h_{in}$ . With the current generation of CPUs, we can perform 64 binary operations in one clock of CPU. The total parameters from the xnorized convolution is  $\frac{1}{64}cN_W N_I + N_I$ , where  $cN_W N_I$  is binary operations,  $N_I$  is non-binary operations. The speed-ratio equation is summarized as Eq.8:

$$S = \frac{cN_W N_I}{\frac{1}{64}cN_W N_I + N_I} \quad (8)$$

In our case, we only compare the operation times of linear projector before DR, since we only binarize this part in **XnODR**. We take  $\mathbf{I}_{Cap}$ , Capsules, as input for linear projector, and  $N_I$  as each capsule's dimension. We also take  $\mathbf{W}_{Cap}$  as related weight, and  $N_W$  as the product of  $dim\_in$  and  $dim\_out$ . Therefore, we formulate the operations of the usual linear projector as Eq.9:

$$caps\_in caps\_out \times dim\_out dim\_in dim\_out, \quad (9)$$

the operations of binary one is formulated as Eq.10:

$$\frac{1}{64} caps\_in caps\_out \times dim\_out dim\_in dim\_out + caps\_out. \quad (10)$$

Therefore, the speed-ratio is :

$$\frac{caps\_in caps\_out dim\_out^2 dim\_in}{\frac{1}{64} caps\_in caps\_out dim\_out^2 dim\_in + dim\_in}. \quad (11)$$

The result is shown in Section.4.

**XnIDR(Xnor Inside Dynamic Routing):** There is Eq.1 within Dynamic Routing. We propose to use binarization as an insert function to simplify Eq.4, such that Eq.12:

$$b_{ij} = b_{ij} + \mathbf{C\_Out}_{j|i} \cdot \mathbf{v}_j \quad (12)$$

where  $\mathbf{v}_j$  has the shape,  $[b, 1, caps\_out, 1, dim\_out]$ ,  $\mathbf{C\_Out}_{j|i}$  has the shape,  $[b, caps\_in, caps\_out, 1, dim\_out]$ . Given that the filter size is easily converted to  $1 \times 1$ , we do not need to do XnorConv here but think out a new way to do xnorized linear projector, which is doing average on the last axis and dot product across all binary filters and scaling filters. We formulate the above as Eq.13:

$$\begin{aligned} \mathbf{C\_Out}_{j|i} \cdot \mathbf{v}_j &\approx (\mathbf{B}_{C\_Out_{j|i}} \otimes \mathbf{B}_{v_j}) \odot \alpha_{C\_Out_{j|i}} \alpha_{v_j} \\ b_{ij} &= b_{ij} + (\mathbf{B}_{C\_Out_{j|i}} \otimes \mathbf{B}_{v_j}) \odot \alpha_{C\_Out_{j|i}} \alpha_{v_j} \end{aligned} \quad (13)$$

$\mathbf{B}_{C\_Out_{j|i}}$  denotes the binary filter of  $\mathbf{C\_Out}_{j|i}$ ,  $\alpha_{C\_Out_{j|i}}$  denotes the scaling factor of  $\mathbf{C\_Out}_{j|i}$ ,  $\mathbf{B}_{v_j}$  denotes the binary filter of  $\mathbf{v}_j$ ,  $\alpha_{v_j}$  denotes the scaling factor of  $\mathbf{v}_j$ .

$C\_Out_{j|i} \cdot v_j$ 's output shape is  $[b, caps\_in, caps\_out, 1, dim\_out]$ , then it gets summed across axis 1. Therefore, the final output shape is  $[b, 1, caps\_out, 1, dim\_out]$  matching with  $b_{ij}$ .

In the meanwhile, we only compare the operation times of linear projector within DR for Speed Up, since we only xnorize this part in **XnIDR**. Here, we use  $C\_Out_{j|i}$  to represent input for linear projector, which is a tensor of capsules, and select  $\hat{v}_j$  to represent weight for the linear projector. Therefore, we formulate the operations of the usual linear projector as Eq.14:

$$caps\_in \times caps\_out \times dim\_out^2, \quad (14)$$

the operations of binary one is formulated as Eq.15:

$$\frac{1}{64} caps\_in \times caps\_out \times dim\_out^2 + dim\_out. \quad (15)$$

The speedration ratio is formulated as Eq.16:

$$\frac{caps\_in \times caps\_out \times dim\_out^2}{\frac{1}{64} caps\_in \times caps\_out \times dim\_out^2 + dim\_out}. \quad (16)$$

The result is shown in Section.4.

**Summary:** There are two linear projectors in the original CapsFCLayer [34]. One is outside DR, while the other is inside DR. XnODR xnorizes the linear projector outside DR. XnIDR xnorizes the one inside DR. Therefore, XnODR and XnIDR simplify operations by xnorizing linear projectors at different positions. However, XnODR causes more information loss than XnIDR, because XnIDR preserves all information in the outer linear projector. If the network implements Xnorization operation on both linear projectors simultaneously, it lacks too much information to predict well. In addition, to reduce the effect of the trade-off between speed and accuracy, we select Linear Transform (LT) and Group Linear Transform (GLT) to calculate linear projector. LT and GLT help switch a broad and shallow network to a narrow and deep one and maintain the same effectiveness or even elevate it. In the meantime, the total parameters get decreased. In general, LT and GLT can relieve trading off between accuracy with speed.

## 4. Experiment

In this section, we firstly introduce the datasets, evaluation metrics, and implementation details. Then, we explain our experiments, present results, and analyze them.

### 4.1. Datasets

We pick both small-scale datasets (MNIST [21], CIFAR-10 [20]) and large-scale datasets (MultiMnist [34]) to validate our proposed XnODR and XnIDR. They would separately work as the only FC layer in the MobileNet V2 [35] (lightweight model) and the ResNet-50 [14] (heavy-weight model) to replace the original dense layers. These variants are to validate XnODR's and XnIDR's effectiveness on those datasets.

**MNIST:** The National Institute of Standards and Technology was in charge of creating the MNIST dataset [21]. It consists of 70,000 28×28 gray-scale images in 10 classes. There are 60,000 training images and 10,000 test images. The American Census Bureau employees contributed to half of the training images, American high school students contributed the other half. So do test images. The categories are 0, 1, 2, 3, 4, 5, 6, 7, 8, and 9.

**CIFAR-10:** This dataset was collected by Alex Krizhevsky, Vinod Nair, and Geoffrey Hinton [20]. It consists of 60,000 32×32 color images in 10 classes, with 6,000 images per class. There are 50,000 training images and 10,000 test images. The categories consist of airplane, automobile, bird, cat, deer, dog, frog, horse, ship, and truck.

**MultiMNIST:** This dataset is generated out of MNIST [21] to prove the effectiveness of CapsNet. Our proposed layers are inspired by CapsNet, therefore, we also validate the XnODR and XnIDR by MultiMNIST [34].

We create MultiMNIST<sup>2</sup> following the instruction from [34], except generating 4 rather than 1K MultiMNIST [34] examples for each digit in the MNIST [21] dataset, because we find that the model can converge to accuracy higher than 99% without a large volume dataset. So the training set consists of 240,000 36×36 gray-scale images in 10 classes, and the test set size is 40,000 36×36 gray-scale images in 10 classes. The categories are 0, 1, 2, 3, 4, 5, 6, 7, 8, and 9.

### 4.2. Evaluation Metrics

This paper takes prediction accuracy (the maximum value among five random training), network parameters, Speed Up, and FLOPs as metrics to evaluate and compare the model performance. Moreover, we would train Networks like ResNet-50 [14], and MobileNet V2 [35] from scratching again to record the metrics used in this paper but missing in the original article.

### 4.3. Implementation Details

We first explain hyperparameters, experiment order, packages' versions, and GPU configuration used in this work.

For the MNIST [21] classification task, we take gray-scale images with the shape of [28, 28, 1] as the input values and convert labels to categorical values with the size of [b, 10].

For the CIFAR-10 [20] classification task, we take color images with the shape of [32, 32, 3] as the input values and convert labels to categorical values with the size of [b, 10]. To enhance the performance, we do random data augmentation on CIFAR-10 [20] before training.

For the MultiMNIST [34] classification task, we take gray-scale images with the shape of [36, 36, 1] as the input values and convert labels to categorical values with the size of [b, 10]. We do not do data augmentation on MultiMNIST [34].

<sup>2</sup>[https://github.com/jiansfogg/CODE-SHOW/blob/master/Python/Multi\\_Mnist/fast\\_generate\\_multimnist.py](https://github.com/jiansfogg/CODE-SHOW/blob/master/Python/Multi_Mnist/fast_generate_multimnist.py)

**Table 1**

Comparison Between All Models Under Different Datasets.

Method	MNIST			CIFAR-10			MultiMNIST		
	Top1	FLOPs	PARA	Top1	FLOPs	PARA	Top2	FLOPs	PARA
Efficient-CapsNet[30]	99.84%	-	161K	-	-	-	94.90%	-	154K
HVCs[5]	99.87%	-	1.5M	89.23%	-	-	-	-	-
PLM(BCE+CB)[9]	-	-	-	70.33%	-	-	89.37%	-	-
CaiT-M-36 U 224[37]	-	-	-	99.40%	53.7B	270.9M	-	-	-
LaNet-L[38]	-	-	-	99.01%	-	44.1M	-	-	-
L1/FC[41]	99.56%	-	-	85.96%	-	-	92.46%	-	-
EnsNet[15]	99.84%	-	-	76.25%	-	-	-	-	-
SCAE[19]	99.0%	-	-	33.48%	-	-	-	-	-
capsnet+PA[42]	99.67%	-	-	85.69%	-	-	94.88%	-	-
CPPN[44]	97.00%	-	-	-	-	-	65.6%	-	-
CapsuleNet[34]	99.65%	-	6.80M	89.40%	-	-	94.8%	-	-
XnorNet[29]	-	-	-	89.83%	-	-	-	-	-
ResNet-50	99.53%	3.86B	26.16M	95.86%	3.86B	26.16M	97.15%	10.08B	26.16M
ResNet_XnODR	99.65%	3.856B	23.86M	96.56%	3.856B	23.86M	99.24%	10.06B	23.86M
ResNet_XnIDR	99.62%	3.856B	23.86M	<b>96.87%</b>	3.856B	23.86M	<b>99.37%</b>	10.06B	23.86M
MobileNet V2	99.50%	314.01M	3.05M	94.64%	314.01M	3.05M	91.77%	92.13M	3.05M
MobileNet_XnODR	<b>99.68%</b>	<b>311.22M</b>	<b>2.99M</b>	95.32%	<b>311.22M</b>	<b>2.99M</b>	97.47%	<b>89.34M</b>	<b>2.99M</b>
MobileNet_XnIDR	99.25%	311.27M	<b>2.99M</b>	95.32%	311.27M	<b>2.99M</b>	97.09%	89.39M	<b>2.99M</b>

Then, to present the convenience and flexibility of XnODR and XnIDR, we decide to insert XnODR and XnIDR into MobileNet V2 [35], a lightweight framework, one by one. Let MobileNet\_XnODR represent MobileNet V2 [35] with XnODR layer, MobileNet\_XnIDR represent MobileNet V2 [35] with XnIDR layer. In the original paper [35], the authors disclosed the experiment results on ImageNet [8], MS-COCO [23], and PASCAL VOC 2012 datasets instead of MNIST, CIFAR-10 [20], and MultiMNIST [34]. Thus, we would validate the original MobileNet V2 [35] on three datasets.

In addition, we also test XnODR and XnIDR on ResNet-50 [14], a heavyweight model. Let ResNet\_XnODR represent ResNet-50 [14] with XnODR layer, ResNet\_XnIDR represent ResNet-50 [14] with XnIDR layer. The authors presented the experiment results on CIFAR-10 [20] from ResNet-44 and ResNet-56 rather than ResNet-50 [14]. They also did not report any experiment results on MNIST [21] and MultiMNIST [34]. Therefore, we take similar steps that we do on MobileNet V2 [35]. We would validate the original ResNet-50 [14] on the above three datasets too.

For all three datasets, we firstly validate MobileNet V2 [35], MobileNet\_XnODR, and MobileNet\_XnIDR. The original MobileNet V2 [35] uses sparse categorical cross-entropy loss function as the cost function, while MobileNet\_XnODR and MobileNet\_XnIDR take marginal loss function as the cost function. All three of them utilize SGD Optimizer and call cyclic learning rate scheduler, where starting learning rate is  $1e-3$ , the ending learning rate is  $1e-9$ , the step size is 6000, and the mode is triangular2.

Then, we start testing ResNet-50 [14], ResNet\_XnODR, and ResNet\_XnIDR. The original ResNet-50 [14] uses

**Table 2**

Speed Comparison Among Proposed Models, ResNet-50 With New Proposed FC Layer and MobileNet V2 New Proposed FC Layer Under Different Datasets.

Models	SpeedUp		
	MNIST	CIFAR-10	MultiMNIST
ResNet_XnODR	63.99	63.99	63.99
ResNet_XnIDR	63.90	63.90	63.98
MobileNet_XnODR	63.98	63.98	63.99
MobileNet_XnIDR	63.80	63.80	63.95

sparse categorical cross-entropy loss function as cost function, while ResNet\_XnODR and ResNet\_XnIDR take marginal loss function as cost function. All three of them utilize SGD Optimizer and call cyclic learning rate scheduler, where the start learning rate is  $1e-3$ , the end learning rate is  $1e-9$ , the step size is 6000, and the mode is triangular2.

In general, we randomly train each model five times to validate the stability. Then, we record the best accuracy, trainable parameters, and FLOPs. We coded the network using Tensorflow (2.2.2) and Keras (2.4.3) framework and ran experiments on the NVIDIA GTX 1080Ti GPUs with 12 GB memory and CUDA Version 10.1.

#### 4.4. Experiment Results

**MNIST:** Our model shows a comparable or even better accuracy with a substantial decrease in the number of parameters. MobileNet\_XnODR achieves the best Top-1 accuracy, 99.68%, on MNIST [21] among our experiments. What's more, it is 0.18% more than MobileNet V2's [35]



Top-1 accuracy, 99.50%. Then, both ResNet\_XnODR's accuracy, 99.65%, and ResNet\_XnIDR's accuracy, 99.62%, are around 0.1% more than the original ResNet-50's [14], 99.53%. In general, ResNet\_XnODR and ResNet\_XnIDR are more stable, they outperform MobileNet\_XnODR and MobileNet\_XnIDR.

On the other side, MobileNet V2's [35] variants, MobileNet\_XnODR and MobileNet\_XnIDR, have 2.99M trainable parameters (the fewest number among all models in the experiment), 60K less than MobileNet V2's [35] 3.05M. Furthermore, variants' FLOPs, 311.22M and 311.27M, are 2.79M and 2.74M less than the original ones, 314.01M. So do ResNet-50 [14], and its variants, ResNet\_XnODR and ResNet\_XnIDR. Both variants have 23.86M trainable parameters, 2.3M less than ResNet-50's [14] 26.16M. Furthermore, both variants' FLOPs, 3.856B, are 4M fewer than the original ones, 3.86B.

As Table.2 shows, the speed of the CNNs main body with XnODR is slightly higher than that with XnIDR. For example, the SpeedUp ratio of MobileNet\_XnODR's xnorized part is 63.98, which is 0.18 higher than that of MobileNet\_XnIDR's, 63.80.

**CIFAR-10:** Our model shows a comparable or even better accuracy with a substantial decrease in the number of parameters. ResNet\_XnIDR achieves the best Top-1 accuracy, 96.87%, on CIFAR-10 [20] among our experiments. What's more, it is 1.01% more than ResNet-50's [14] Top-1 accuracy, 95.86%. It outperforms ResNet\_XnODR on CIFAR-10 [20] because ResNet\_XnODR's Top-1 accuracy is just 0.7% more than the original one's. So does MobileNet\_XnIDR, which accuracy is 95.38%. It is 0.06% more than MobileNet\_XnODR's accuracy, 95.32%. Then both of their accuracies are around 0.72% more than the original MobileNet V2's [35], 94.64%. In general, ResNet\_XnODR and ResNet\_XnIDR outperform MobileNet\_XnODR and MobileNet\_XnIDR again.

On the other side, the MobileNet V2 [35] requires the input image size should be at least 32×32. We enlarge the MNIST's [21] image size from 28×28 to 32×32 on the last experiment. Thus, the test on the MNIST [21] has the identical input image size as that on the CIFAR-10 [20]. It means that the trainable parameters and FLOPs of MobileNet V2 [35], and its variants, MobileNet\_XnODR and MobileNet\_XnIDR, stay the same as well. So does ResNet-50 [14]. It also requires that the input size should be more than 32×32.

As Table.2 shows, the speed of the CNNs main body with XnODR is slightly higher than that with XnIDR. For example, the SpeedUp ratio of ResNet\_XnODR's xnorized part is 63.99, which is 0.09 more than that of ResNet\_XnIDR's, 63.90.

**MultiMNIST:** Our model shows a comparable or even better accuracy with a substantial decrease in the number of parameters. ResNet\_XnIDR achieves the best Top-2 accuracy, 99.37%, on MultiMNIST [34] among our experiments. It is 2.22% more than ResNet-50's [14] Top-2 accuracy, 97.15%. It outperforms ResNet\_XnODR on

**Table 3**

Experiment Results On CIFAR-10 From Cited Papers.

Models	CIFAR-10 Accuracy
Aff-CapsNets [12]	76.28
CapsNetSIFT [25]	91.27
HGCNet-91 [40]	94.47
Ternary connect + Quantized backprop [24]	87.99
Greedy Algorithm for Quantizing [28]	88.88
SLB on ResNet20 [43]	92.1
SLB on VGG small [43]	94.1
DoReFa-Net on VGG-11 [13]	86.30
DoReFa-Net on ResNet14 [13]	89.84

MultiMNIST [34] because ResNet\_XnODR's Top-2 accuracy is merely 2.09% more than the original one's. Then, MobileNet\_XnODR's Top-2 accuracy, 97.47%, is 6.2% over MobileNet V2's, 91.77%. It also outperforms MobileNet\_XnIDR's, 97.09%, which is 5.8% more than the original ResNet-50's [14]. In general, ResNet\_XnODR and ResNet\_XnIDR outperform MobileNet\_XnODR and MobileNet\_XnIDR again.

On the other hand, MobileNet\_XnODR costs the fewest FLOPs, 89.34M. Both MobileNet\_XnODR and MobileNet\_XnIDR have around 2.79M less FLOPs than MobileNet V2. They also have 2.99M trainable parameters, 60K less than the original ones, 3.05M. If we look at the heavyweight model, ResNet-50 [14], and its variants, ResNet\_XnODR and ResNet\_XnIDR, both variants have 23.86M trainable parameters, 2.3M less than ResNet-50's [14] 26.16M. Furthermore, both variants' FLOPs, 10.06B, are around 2M less than the original ones, 10.08B.

As Table.2 shows, the speed of the CNNs main body with XnODR is slightly higher than that with XnIDR. For example, the SpeedUp ratio of MobileNet\_XnODR's xnorized part is 63.99, which is 0.01 more than that of MobileNet\_XnIDR's, 63.98.

## 4.5. Analysis and Evaluation

### 4.5.1. Speed Analysis

Eq.8 is the speedup function, which lets the number of operations in original convolution divide by that of operations in XnorConv. As a ratio, it reflects the multiple of MADD spent by the usual convolution over XnorConv.

According to Table.2, Xnorization helps speed up around 64 times on linear projector in XnODR under all three datasets, so does XnIDR. We also showed that the speedup of the linear projector in XnIDR is a little less than XnODR in Section.4.4. Additionally, MobileNet\_XnODR has less FLOPs than MobileNet\_XnIDR, so does ResNet\_XnODR. The reason is that the binarized input values and weights in XnIDR are in the iteration structure, while those in XnODR are out of the loop, which results in XnODR's slightly better performance on speeding the specific operations and causing less FLOPs. Therefore, the CNNs' main body with XnODR can run faster than that with XnIDR.

#### 4.5.2. Comprehensive Analysis

Albeit, ResNet\_XnIDR has the number of trainable parameters as ResNet\_XnODR, it costs slightly more FLOPs than ResNet\_XnODR across all three datasets and reaches better accuracy on the complex dataset, CIFAR-10 [20], than ResNet\_XnODR.

The experiment on MobileNet V2 [35] also supports this view. Compared with the original MobileNet V2, MobileNet\_XnODR and MobileNet\_XnIDR reach better accuracy by costing fewer FLOPs and parameters, especially on CIFAR-10 [20] and MultiMNIST [34]. What's more, either MobileNet\_XnODR, MobileNet\_XnIDR, ResNet\_XnODR, or ResNet\_XnIDR achieves better accuracy than any models in Table.3 because the accuracy from cited papers is under 95%.

In general, ResNet\_XnODR and ResNet\_XnIDR achieve better performance with less FLOPs and parameters among all three datasets.

The reason is that the DR mechanism helps improve the prediction results while Xnorization helps reduce the parameter and speed the calculation process. Hence, our proposed XnODR and XnIDR suit both lightweight models and heavyweight models.

At the same time, MobileNet\_XnODR and ResNet\_XnODR have larger speedup ratio and less FLOPs than MobileNet\_XnIDR and ResNet\_XnIDR, but MobileNet\_XnODR's accuracy and ResNet\_XnODR's are comparable to MobileNet\_XnIDR's accuracy and ResNet\_XnIDR's. However, CNNs main body with XnIDR achieves better accuracy than CNNs main body with XnODR on the complex dataset, CIFAR-10 [20]. We weigh complex datasets more than simple ones. After comprehensively consideration, we state that CNNs main body with XnIDR is better than CNNs main body with XnODR.

In XnODR and XnIDR, the hyperparameters are batch size, input capsule number, and output capsule number, which subjects to dataset number, the size of input images, and dataset's category number. It is less necessary to tune them to strengthen the rationality of our work. Hence, we skip the ablation study.

## 5. Discussion

The CNNs main body with our proposed FC layers (XnODR and XnIDR) demonstrate that they outperform the original models both in terms of accuracy and speed by their solid performance in our experiments. For example, ResNet\_XnODR and ResNet\_XnIDR achieve over 96.5% accuracy with the cost of 3.856B FLOPs and 23.86M parameters on CIFAR-10 [20] while ResNet-50 [14] returns accuracy lower than 96% with more FLOPs and parameters. As we can see, fusing xnorization into the DR mechanism helps speed the model while maintaining a comparable or even better accuracy. Hence, we can implement XnODR and XnIDR as effective FC layers in both lightweight and heavyweight models. In order to improve the network's representative capability, either XnODR or XnIDR can work

as a parallel branch in CNNs to provide rotation invariance, increase the accuracy and avoid over time-consuming. In addition, it is helpful to load its output into relabeling mechanism as a contrast. However, we do not validate our method on large-scale complex datasets such as ImageNet [8] yet, but only validate them on small-scale complex datasets such as CIFAR-10 [20]. Specifically, while using the Xnorization method, the network is less likely to do a comparable performance on complex datasets due to losing too much information, such as a less satisfying performance on ImageNet [8] in [29]. In the meanwhile, Sabour *et al.* presented the CapsConv layer with EM routing in [33], which is already validated work on CIFAR-10 [20]. Hence, the next step is to create a new Xnorization method and avoid over information loss. And we would modify the XnODR and XnIDR by this new method, utilize this method in the CapsConv layer [33] to create the XnorCapsConv layer and build a new network with XnorCapsConv layer and XnODR or XnIDR. The target is to achieve good performance on large-scale complex datasets such as AffectNet [31] and ImageNet [8].

## 6. Conclusion and Future Work

High accuracy and fast processing speed are two highlights of CapsuleNet and XnorNet. Combining these two advantages helps the network to speed the training while maintaining good or even better performance. Inspired by this idea, we propose XnODR and XnIDR, the alternative options for the usual FC layer. Then, we inserted them into the MobileNet V2 [35] and ResNet-50 [14] and experimented on three datasets, MNIST [21], CIFAR-10 [20], and MultiMnist [34]. The result shows that the main body with either XnODR or XnIDR takes less parameters and less FLOPs than the original one. And the variants reach higher accuracy. We expect that XnODR and XnIDR can be supplementary branches on the complex classification task. In the future, we would work on creating a new Xnorization algorithm to calculate sign and scaling factors and avoid overly information loss. As a future work we will fuse this new Xnorization method and EM Routing to create a new xnorized CapsConv layer.

## References

- [1] Arora, S., Bhaskara, A., Ge, R., Ma, T., 2014. Provable bounds for learning some deep representations, in: Xing, E.P., Jebara, T. (Eds.), Proceedings of the 31st International Conference on Machine Learning, PMLR, Beijing, China. pp. 584–592.
- [2] Ba, L.J., Caruana, R., 2014. Do deep nets really need to be deep?, in: Proceedings of the 27th International Conference on Neural Information Processing Systems - Volume 2, MIT Press, Cambridge, MA, USA. pp. 2654–2662.
- [3] Bahadori, M.T., 2018. Spectral capsule networks.
- [4] Bulat, A., Tzimiropoulos, G., 2019. Xnor-net++: Improved binary neural networks, in: BMVC.
- [5] Byerly, A., Kalganova, T., Dear, I., 2021. No routing needed between capsules. Neurocomputing 463, 545–553. doi:<https://doi.org/10.1016/j.neucom.2021.08.064>.

- [6] Cybenko, G., 1989. Approximation by superpositions of a sigmoidal function. *Mathematics of Control, Signals, and Systems (MCSS)* 2, 303–314. URL: <http://dx.doi.org/10.1007/BF02551274>, doi:10.1007/BF02551274.
- [7] Dauphin, Y., Bengio, Y., 2013. Big neural networks waste capacity. *CoRR* abs/1301.3583.
- [8] Deng, J., Dong, W., Socher, R., Li, L.J., Li, K., Fei-Fei, L., 2009. Imagenet: A large-scale hierarchical image database, in: 2009 IEEE Conference on Computer Vision and Pattern Recognition, pp. 248–255. doi:10.1109/CVPR.2009.5206848.
- [9] Duarte, K., Rawat, Y., Shah, M., 2021. Plm: Partial label masking for imbalanced multi-label classification, in: Proceedings of the IEEE/CVF Conference on Computer Vision and Pattern Recognition (CVPR) Workshops, pp. 2739–2748.
- [10] Floropoulos, N., Tefas, A., 2019. Complete vector quantization of feedforward neural networks. *Neurocomputing* 367, 55–63. doi:<https://doi.org/10.1016/j.neucom.2019.08.003>.
- [11] Gong, Y., Liu, L., Yang, M., Bourdev, L., 2014. Compressing Deep Convolutional Networks using Vector Quantization. *arXiv e-prints*, arXiv:1412.6115arXiv:1412.6115.
- [12] Gu, J., Tresp, V., 2020. Improving the robustness of capsule networks to image affine transformations. 2020 IEEE/CVF Conference on Computer Vision and Pattern Recognition (CVPR), 7283–7291.
- [13] Guerra, L., Zhuang, B., Reid, I., Drummond, T., 2020. Automatic Pruning for Quantized Neural Networks. *arXiv e-prints*, arXiv:2002.00523arXiv:2002.00523.
- [14] He, K., Zhang, X., Ren, S., Sun, J., 2016. Deep residual learning for image recognition. 2016 IEEE Conference on Computer Vision and Pattern Recognition (CVPR), 770–778.
- [15] Hirata, D., Takahashi, N., 2020. Ensemble learning in CNN augmented with fully connected subnetworks. *arXiv e-prints*, arXiv:2003.08562arXiv:2003.08562.
- [16] Hwang, K., Sung, W., 2014. Fixed-point feedforward deep neural network design using weights +1, 0, and -1, in: 2014 IEEE Workshop on Signal Processing Systems (SiPS), pp. 1–6. doi:10.1109/SiPS.2014.6986082.
- [17] Iandola, F.N., Han, S., Moskewicz, M.W., Ashraf, K., Dally, W.J., Keutzer, K., 2016. SqueezeNet: AlexNet-level accuracy with 50x fewer parameters and <0.5MB model size. *arXiv e-prints*, arXiv:1602.07360arXiv:1602.07360.
- [18] Kim, J., Jang, S., Park, E., Choi, S., 2020. Text classification using capsules. *Neurocomputing* 376, 214–221.
- [19] Kosiorek, A.R., Sabour, S., Teh, Y.W., Hinton, G., 2019. Stacked capsule network autoencoders, in: *Neural Information Processing Systems*. URL: <https://arxiv.org/pdf/1906.06818.pdf>.
- [20] Krizhevsky, A., Nair, V., Hinton, G., . *Cifar-10 (canadian institute for advanced research)* URL: <http://www.cs.toronto.edu/~kriz/cifar.html>.
- [21] LeCun, Y., Cortes, C., 2010. MNIST handwritten digit database URL: <http://yann.lecun.com/exdb/mnist/>.
- [22] Lenssen, J.E., Fey, M., Libuschewski, P., 2018. Group equivariant capsule networks, in: *NeurIPS*, pp. 8858–8867.
- [23] Lin, T.Y., Maire, M., Belongie, S., Hays, J., Perona, P., Ramanan, D., Dollár, P., Zitnick, C.L., 2014. Microsoft coco: Common objects in context, in: Fleet, D., Pajdla, T., Schiele, B., Tuytelaars, T. (Eds.), *Computer Vision – ECCV 2014*, Springer International Publishing, Cham. pp. 740–755.
- [24] Lin, Z., Courbariaux, M., Memisevic, R., Bengio, Y., 2016. Neural networks with few multiplications, in: Bengio, Y., LeCun, Y. (Eds.), 4th International Conference on Learning Representations, ICLR 2016, San Juan, Puerto Rico, May 2–4, 2016, Conference Track Proceedings. URL: <http://arxiv.org/abs/1510.03009>.
- [25] Lin, Z., Gao, W., Jia, J., Huang, F., 2021a. Capsnet meets sift: A robust framework for distorted target categorization. *Neurocomputing* 464, 290–316. doi:<https://doi.org/10.1016/j.neucom.2021.08.087>.
- [26] Lin, Z., Jia, J., Huang, F., Gao, W., 2021b. A coarse-to-fine capsule network for fine-grained image categorization. *Neurocomputing* 456, 200–219. doi:<https://doi.org/10.1016/j.neucom.2021.05.032>.
- [27] Liu, Z., Luo, W., Wu, B., Yang, X., Liu, W., Cheng, K., 2019. Bi-real net: Binarizing deep network towards real-network performance. *International Journal of Computer Vision* 128, 202–219.
- [28] Lybrand, E., Saab, R., 2020. A Greedy Algorithm for Quantizing Neural Networks. *Journal of Machine Learning Research*, arXiv:2010.15979arXiv:2010.15979.
- [29] M. Rastegari, V. Ordonez, J.R., Farhadi, A., 2016. Xnor-net: Imagenet classification using binary convolutional neural networks, in: *European Conference on Computer Vision (ECCV)*, Springer. pp. 525–542.
- [30] Mazzia, V., Salvetti, F., Chiaberge, M., 2021. Efficient-capsnet: Capsule network with self-attention routing. *Scientific Reports* 11.
- [31] Mollahosseini, A., Hasani, B., Mahoor, M.H., 2019. Affectnet: A database for facial expression, valence, and arousal computing in the wild. *IEEE Transactions on Affective Computing* 10, 18–31.
- [32] Ribeiro, F., Leontidis, G., Kollias, S., 2019. Capsule routing via variational bayes, pp. 1–8. URL: <https://aaai.org/Conferences/AAAI-20/>, doi:10.1609/aaai.v34i04.5785. 34th AAAI 2020 Accepted Paper - Flagship/Top conference with very high h-index; Thirty-Fourth AAAI Conference on Artificial Intelligence, AAAI ; Conference date: 07-02-2020 Through 12-02-2020.
- [33] S. Sabour, G.E.H., Frosst, N., 2018. Matrix capsules with em routing, in: *International Conference on Learning Representations (ICLR)*.
- [34] S. Sabour, N.F., Hinton, G.E., 2017. Dynamic routing between capsules., in: *Neural Information Processing Systems (NIPS)*.
- [35] Sandler, M., Howard, A.G., Zhu, M., Zhmoginov, A., Chen, L.C., 2018. Mobilenetv2: Inverted residuals and linear bottlenecks. 2018 IEEE/CVF Conference on Computer Vision and Pattern Recognition, 4510–4520.
- [36] Szegedy, C., Liu, W., Jia, Y., Sermanet, P., Reed, S., Anguelov, D., Erhan, D., Vanhoucke, V., Rabinovich, A., 2015. Going deeper with convolutions, in: 2015 IEEE Conference on Computer Vision and Pattern Recognition (CVPR), pp. 1–9. doi:10.1109/CVPR.2015.7298594.
- [37] Touvron, H., Cord, M., Sablayrolles, A., Synnaeve, G., Jégou, H., 2021. Going deeper with Image Transformers. *arXiv e-prints*, arXiv:2103.17239arXiv:2103.17239.
- [38] Wang, L., Xie, S., Li, T., Fonseca, R., Tian, Y., 2019. Sample-Efficient Neural Architecture Search by Learning Action Space. *arXiv e-prints*, arXiv:1906.06832arXiv:1906.06832.
- [39] Xi, E., Bing, S., Jin, Y., 2017. Capsule Network Performance on Complex Data. *arXiv e-prints*, arXiv:1712.03480arXiv:1712.03480.
- [40] Xie, X., Zhou, Y., Kung, S.Y., 2020. Exploring highly efficient compact neural networks for image classification, in: 2020 IEEE International Conference on Image Processing (ICIP), pp. 2930–2934. doi:10.1109/ICIP40778.2020.9191334.
- [41] Yang, H., Li, S., Yu, B., 2021. Routing Towards Discriminative Power of Class Capsules. *arXiv e-prints*, arXiv:2103.04278arXiv:2103.04278.
- [42] Yang, Z., Wang, X., 2019. Reducing the dilution: An analysis of the information sensitiveness of capsule network with a practical improvement method. *arXiv e-prints*, arXiv:1903.10588arXiv:1903.10588.
- [43] Yang, Z., Wang, Y., Han, K., Xu, C., Xu, C., Tao, D., Xu, C., 2020. Searching for Low-Bit Weights in Quantized Neural Networks. *arXiv e-prints*, arXiv:2009.08695arXiv:2009.08695.
- [44] Yao, H., Regan, M., Yang, Y., Ren, Y., 2019. Image decomposition and classification through a generative model, in: 2019 IEEE International Conference on Image Processing, ICIP 2019 - Proceedings, IEEE Computer Society. pp. 400–404. doi:10.1109/ICIP.2019.8802991. publisher Copyright: © 2019 IEEE.; 26th IEEE International Conference on Image Processing, ICIP 2019 ;



Conference date: 22-09-2019 Through 25-09-2019.

- [45] Yoshida, Y., Oiwa, R., Kawahara, T., 2018. Ternary sparse xnor-net for fpga implementation, in: 2018 7th International Symposium on Next Generation Electronics (ISNE), pp. 1–2. doi:10.1109/ISNE.2018.8394728.
- [46] Yu, D., Seide, F., Li, G., 2012. Conversational speech transcription using context-dependent deep neural networks, in: Proceedings of the 29th International Conference on International Conference on Machine Learning, Omnipress, Madison, WI, USA. pp. 1–2.
- [47] Zhu, S., Duong, L.H.K., Liu, W., 2020. Xor-net: An efficient computation pipeline for binary neural network inference on edge devices, in: 2020 IEEE 26th International Conference on Parallel and Distributed Systems (ICPADS), pp. 124–131. doi:10.1109/ICPADS51040.2020.00026.

## A. Xnorization

Xnorization is to split the tensor into 2 parts. One is sign, the other one is scaling factor.

Let  $\mathcal{I}$  be a set of tensors. And  $\mathbf{I} = \mathcal{I}_{l(l=1,\dots,L)}$ ,  $\mathbf{I} \in \mathbb{R}^{c \times w_{in} \times h_{in}}$  represents the input tensor for the  $l^{th}$  layer of network, where  $(c, w_{in}, h_{in})$  means *channel*, *width* and *height*. We split the tensor  $\mathbf{I}$  into two values, binary filter  $\mathbf{B} \in \{+1, -1\}^{c \times w_{in} \times h_{in}}$  and scaling factor  $\alpha \in \mathbb{R}^+$ , and use them to estimate  $\mathbf{I} \approx \alpha \mathbf{B}$ .

We first discuss the Sign and the binary filter. According to [29]  $k$ -bit Quantization is  $q_k(x) = 2(\frac{[(2^k-1)(\frac{x+1}{2})]}{2^k-1} - \frac{1}{2})$ . The sign function is 1-bit Quantization, such that  $q_1(x) = 2(\frac{[(2^1-1)(\frac{x+1}{2})]}{2^1-1} - \frac{1}{2}) = 2(\frac{x+1}{2} - \frac{1}{2})$ , where the inner function,  $\frac{x+1}{2}$ , is Hard Sigmoid function, the outer function,  $2(Y - \frac{1}{2})$ , is Tanh function. Therefore, the sign function can be formulated as shown in the Eq.17

$$\begin{aligned} \mathbf{B}_{HS} &= \text{Hard\_Sigmoid}(\text{Round}(\mathbf{I}_{\text{Norm}})) \\ &= \frac{\text{Round}(\mathbf{I}_{\text{Norm}}) + 1}{2} \end{aligned} \quad (17)$$

where  $\mathbf{B}_{HS}$  is the output of Hard Sigmoid,  $\mathbf{I}_{\text{Norm}}$  is the Min-Max Normalization result of  $\mathbf{I}$ . Its range is  $[0, 1]$ . Round function will round value bigger than 0.5 to be 1, less than or equal to 0.5 to be 0. And it leaves  $\mathbf{I}_{\text{Norm}}$  only 2 values, 0 and 1 after rounding, then the output of Hard Sigmoid function  $\mathbf{B}_{HS} \in \{0.5, 1\}$ . To control the value of  $\mathbf{B}_{HS}$  between 0 and 1, we call Clip function and round its output, such that

$$\begin{aligned} \mathbf{B}_C &= \text{Clip}(\mathbf{B}_{HS}) = \max(0, \min(1, \mathbf{B}_{HS})) \\ \mathbf{B}_R &= \text{Round}(\mathbf{B}_C). \end{aligned} \quad (18)$$

Therefore, we get  $\mathbf{B}_R$ , which only has 2 values, 0 and 1. To get the expected binary filter  $\mathbf{B}$ , we load  $\mathbf{B}_R$  into Tanh function,  $\mathbf{B} = \text{Tanh}(\mathbf{B}_R) = 2 \times \mathbf{B}_C - 1 \in \{-1, +1\}$ . Now, we calculate the sign of  $\mathbf{I}$  out.

About scaling factor, according to [29], we use the average of  $\mathbf{I}$  to represent it.

$$\alpha = \frac{1}{n}(\mathbf{I}^T \mathbf{B}) = \frac{\sum |\mathbf{I}_i|}{n} = \frac{1}{n} \|\mathbf{I}\|_{L_1} \quad (L1 - Norm) \quad (19)$$

Eq.19 is the formula to get scaling factor, where  $\alpha$  represents the scaling factor. Xnorization is the core of XnorConvLayer, which is reviewed below.

## B. XnorConvLayer

XnorConvLayer is similar to the standard Conv layer, except xnorizing input and weight before doing convolution. Therefore, XnorConvLayer has xnorized input values and xnorized weights. We formulate it as the following.

Let  $\mathbf{I}_j$  denote  $j^{th}$  tensor of  $\mathbf{I}$ ,  $\alpha_{\mathbf{I}_j}$  denote  $j^{th}$  scaling factor,  $\mathbf{B}_1$  denote binary filter of  $\mathbf{I}$ . Then  $\mathbf{I} \approx \mathbf{A}_1 \mathbf{B}_1$  is the estimate of  $\mathbf{I}$  after xnorize, where  $\mathbf{A}_1 = \{\alpha_{\mathbf{I}_0}, \alpha_{\mathbf{I}_1}, \dots, \alpha_{\mathbf{I}_{h_{in}}}\}$ .

Then, let  $\mathcal{W}$  be a set of tensors, and  $\mathbf{W}$  represent the  $k^{th}$  weight filter in the  $l^{th}$  layer of the network such that  $\mathbf{W} = \mathcal{W}_{lk(k=1,\dots,K^l)}$ .  $K^l$  is the number of weight filters in the  $l^{th}$  layer of the network. What's more,  $\mathbf{W} \in \mathbb{R}^{c \times w \times h}$ , where  $w \leq w_{in}$ ,  $h \leq h_{in}$ .

Next, we start estimating  $\mathbf{W}$  with binary filter,  $\mathbf{B}_W$ , and scaling filter,  $\mathbf{A}_W$ , such that  $\mathbf{W} \approx \mathbf{A}_W \mathbf{B}_W$ .

$\mathbf{A}_W = \{\alpha_{W_0}, \alpha_{W_1}, \dots, \alpha_{W_j}, \dots, \alpha_{W_{h_{in}}}\}$ , where  $\alpha_{W_j}$  denote  $j^{th}$  scaling factor.

According to XNOR-Net [29], Xnorization replaces multiplication in convolutional operations with additions and subtractions. And it causes 58× faster convolutional operations and 32× memory savings. This process is called **Binary Dot Product**.

To approximate the dot product between  $\mathbf{X}_1$  and  $\mathbf{X}_2$ , such that  $\mathbf{X}_1^T \mathbf{X}_2 \approx \alpha_1 \mathbf{B}_1^T \alpha_2 \mathbf{B}_2$ , where  $\mathbf{B}_1, \mathbf{B}_2 \in \{+1, -1\}^n$ ,  $\alpha_1, \alpha_2 \in \mathbb{R}^+$ , the paper solved and proved the following optimization:

$$\alpha_1^*, \mathbf{B}_1^*, \alpha_2^*, \mathbf{B}_2^* = \underset{\alpha_1, \mathbf{B}_1, \alpha_2, \mathbf{B}_2}{\text{argmin}} \|\mathbf{X}_1 \odot \mathbf{X}_2 - \alpha_1 \alpha_2 \mathbf{B}_1 \odot \mathbf{B}_2\| \quad (20)$$

where  $\odot$  represents element-wise product.

In the meanwhile, for input tensors,  $\mathbf{I}$ , and weight,  $\mathbf{W}$ , we need to compute scaling factor,  $\alpha_{\mathbf{I}_j}$ , for all possible sub-tensors in  $\mathbf{I}$  with same size as  $\mathbf{W}$  during convolution. To overcome the redundant computations caused by overlaps between sub-tensors, the paper firstly computed a matrix  $\mathbf{M}_I = \frac{\sum |\mathbf{I}_{:,c}|}{c}$ , which is the average over absolute values of the elements in the input  $\mathbf{I}$  across the channel,  $c$ . Then the paper convolved  $\mathbf{M}_I$  with a 2D filter  $\mathbf{k} \in \mathbb{R}^{w \times h}$ ,  $\mathbf{A}_I = \mathbf{M}_I * \mathbf{k}$ , where  $\forall i, j \mathbf{k}_{ij} = \frac{1}{w \times h}$  and  $*$  is a convolutional operation.  $\mathbf{A}_I$  contains scaling factors  $\alpha_{\mathbf{I}_j}$  for all sub-tensors in the input  $\mathbf{I}$ .

The above description proves that it makes sense to estimate  $\mathbf{I} * \mathbf{W}$  by  $(\mathbf{B}_I \otimes \mathbf{B}_W) \odot \mathbf{A}_I \alpha_W$ , which can be formulated as Eq.21:

$$\mathbf{I} * \mathbf{W} \approx (\mathbf{B}_I \otimes \mathbf{B}_W) \odot \mathbf{A}_I \alpha_W \quad (21)$$

where  $\otimes$  denotes the convolutional operation using XNOR and the bitcount operations.